



# Complex I, V, and MDH2 deficient human skin fibroblasts reveal distinct metabolic signatures by $^1\text{H}$ HR-MAS NMR

Christoph Meyer<sup>1,2,3</sup>  | Damian Hertig<sup>1,2</sup>  | Janine Arnold<sup>1,2</sup> |  
 Christian Urzi<sup>1,2,3</sup> | Sandra Kurth<sup>2</sup> | Johannes A. Mayr<sup>4</sup> |  
 André Schaller<sup>5</sup> | Peter Vermathen<sup>1</sup>  | Jean-Marc Nuoffer<sup>2,6</sup> 

<sup>1</sup>Magnetic Resonance Methodology, Institute of Diagnostic and Interventional Neuroradiology, University of Bern, Bern, Switzerland

<sup>2</sup>Institute of Clinical Chemistry, University Hospital Bern, Bern, Switzerland

<sup>3</sup>Graduate School for Cellular and Biomedical Sciences, University of Bern, Bern, Switzerland

<sup>4</sup>Department of Pediatrics, Paracelsus Medical University, Salzburg, Austria

<sup>5</sup>Department of Human Genetics, Inselspital, Bern University Hospital, University of Bern, Bern, Switzerland

<sup>6</sup>Department of Pediatric Endocrinology, Diabetology and Metabolism, University Children's Hospital of Bern, Bern, Switzerland

## Correspondence

Jean-Marc Nuoffer, Inselspital Bern, Zentrum für Seltene Krankheiten, INO F, Freiburgstrasse, CH-3010 Bern, Switzerland.  
 Email: [jean-marc.nuoffer@insel.ch](mailto:jean-marc.nuoffer@insel.ch)

## Funding information

Schweizerischer Nationalfonds zur Förderung der Wissenschaftlichen Forschung, Grant/Award Number: 192691

**Communicating Editor:** John Christodoulou

## Abstract

In this study, we investigated the metabolic signatures of different mitochondrial defects (two different complex I and complex V, and the one *MDH2* defect) in human skin fibroblasts (HSF). We hypothesized that using a selective culture medium would cause defect specific adaptation of the metabolome and further our understanding of the biochemical implications for the studied defects. All cells were cultivated under galactose stress condition and compared to glucose-based cell culture condition. We investigated the bioenergetic profile using Seahorse XFe96 cell analyzer and assessed the extracellular metabolic footprints and the intracellular metabolic fingerprints using NMR. The galactose-based culture condition forced a bioenergetic switch from a glycolytic to an oxidative state in all cell lines which improved overall separation of controls from the different defect groups. The extracellular metabolome was discriminative for separating controls from defects but not the specific defects, whereas the intracellular metabolome suggests CI and CV changes and revealed clear *MDH2* defect-specific changes in metabolites associated with the TCA cycle, malate aspartate shuttle, and the choline metabolism, which are pronounced under galactose condition.

## KEYWORDS

CI, CV, galactose, MDH2, mitochondrial dysfunction, NMR

Peter Vermathen and Jean-Marc Nuoffer contributed equally.

This is an open access article under the terms of the [Creative Commons Attribution-NonCommercial-NoDerivs](https://creativecommons.org/licenses/by-nc-nd/4.0/) License, which permits use and distribution in any medium, provided the original work is properly cited, the use is non-commercial and no modifications or adaptations are made.

© 2023 The Authors. *Journal of Inherited Metabolic Disease* published by John Wiley & Sons Ltd on behalf of SSIEM.

## 1 | INTRODUCTION

Mitochondrial disorders are among the most frequent inborn errors of metabolism. Different defects are clinically heterogeneous, the pathomechanisms are not

well understood and frequently lack specific metabolic markers.<sup>1</sup> Mitochondria not only hold an important role in energy production via oxidative phosphorylation (OXPHOS) but also are involved in many signaling pathways and biosynthesis.<sup>2</sup> Therefore, defects within the mitochondrial metabolism may lead to highly diverse metabolic changes including numerous secondary effects, for example through alterations of the redox state across the inner mitochondrial membrane, or imbalances in the mitochondrial proteostasis (resulting in the mitochondrial unfolded protein response<sup>3</sup>). Furthermore, changes in TCA cycle metabolite levels can have a myriad of downstream effects as many biochemical reactions and mitochondrial shuttles are governed by negative feedback loops. The release of mitochondrial reactive oxygen species (ROS) has been described in complex I (CI) and complex V (CV) defects to result in metabolic adaptations.<sup>4–6</sup>

The cell metabolism and especially the mitochondrial function and dysfunction is dependent on nutrient availability and galactose-based fibroblast culture media has been used as screening test of OXPHOS deficient cell lines. Galactose based culture decreases activity of anaerobic glycolysis and induces aerobic energy production.<sup>7</sup> It has been shown that galactose based media led to an increase in mitochondrial oxidative metabolism and better discriminating metabolic signatures in mitochondrial dysfunctions.<sup>8</sup>

In a previous paper we have shown that metabolomics discrimination between a CI and a pyruvate dehydrogenase (PDH) defect can be ameliorated using galactose based media.<sup>9</sup> The CI defect showed increased choline metabolites under galactose while the PDH defect displayed a heightened glutaminolytic metabolism and an increase of several amino acids (leucine, isoleucine, valine, phenylalanine, and tyrosine) when compared to controls.

We were curious whether the metabolic profiles of even structurally nearby defects within the respiratory chain such as complex I (CI; *NDUFS3* and *NDUFS4*) and complex V (CV; *MT-ATP6* and *MT-ATP8/6*) were distinguishable from each other and from the *MDH2* (mitochondrial malate dehydrogenase) associated TCA cycle defect using NMR based metabolomics. NMR spectroscopy is an established technique in the field of metabolomics for ex vivo applications. The most common use is for biofluids using liquid NMR,<sup>10</sup> however, High-Resolution Magic Angle Spinning (HR-MAS) NMR is capable of generating metabolic profiles of cells and biopsies without the need for metabolite extraction or tissue homogenization. The resulting measurements are, therefore, closer to in vivo conditions than other methods. By spinning semi-solid samples at the magic angle of 54.7° relative to  $B_0$  several line broadening effects are averaged out. The resulting spectral quality regarding both

## Synopsis

The intracellular metabolome suggests CI and CV changes and revealed clear *MDH2* defect-specific changes in metabolites associated with the TCA cycle, malate aspartate shuttle and the choline metabolism.

resolution and sensitivity is comparable to liquid NMR samples.<sup>11–13</sup>

We hypothesize that the different biochemical defects generate different metabolic signaling in dysfunction. Studying the metabolic impact of different mitochondrial defects can help identify and characterize signaling cascades caused by defects and, therefore, help to reveal yet unknown relationships between mitochondrial dysfunction and secondary metabolic alterations.

## 2 | MATERIALS AND METHODS

### 2.1 | Cell culture

We studied HSF cell lines derived from three controls, two patients with complex I (CI; homozygous variants: NM\_004551.3(*NDUFS3*):c.595C>T p.(Arg199Trp), NM\_002495.4(*NDUFS4*):c.462del p.(Lys154fs)), two patients with complex V (CV; mitochondrially encoded variants: NC\_012920.1(*MT-ATP6*):m.9134A>G, heteroplasmic: 82%, NC\_012920.1:(*MT-ATP6/8*):m.8528T>C, homoplasmic) deficiency and one patient with malate dehydrogenase deficiency (*MDH2*; compound heterozygous missense variants: NM\_005918.4(*MDH2*): c.[398C>T]; [445delinsACA], p.[(Pro133Leu)];[(Pro149Hisfs\*22)]). This particular *MDH2* deficient cell line was previously published within the scope of a triheptanoin treatment, but never with the methods published in this paper.<sup>14</sup> Enzymatic activity assays, 82% heteroplasmy rate for *MT-ATP6*, homoplasmy for *MT-ATP6/8* and oximetric analysis confirmed the genetic defects as pathological (Table S1). The cell lines stem from skin biopsies that were collected for diagnostic purposes. For each cell line, at least three biological replicates were cultured for both culture conditions. As previously described,<sup>9</sup> cells were cultured in minimal essential medium (MEM; Gibco Carlsbad, CA) with the following additional supplements: 25 mM glucose, 10% foetal calf serum (FCS), 2 mM L-glutamine, 1 mM sodium pyruvate, 200 μM uridine, 1× non-essential amino acids (100 μM glycine, L-alanine, L-asparagine, L-aspartic acid, L-glutamic acid, L-proline, and L-serine), 100 U/mL penicillin,

100 µg/mL streptomycin, and 10 µg/mL chlortetracycline. FB were cultured at 37°C in a humidified 5% CO<sub>2</sub> cell culture incubator and were passaged using 0.05% trypsin–EDTA. Cell numbers were determined in a Neubauer hemacytometer using trypan blue exclusion method. For metabolic investigations, cells were washed once with phosphate buffered saline (PBS, pH 7.4) and cultivated for 18 h in Dulbecco's Modified Eagle Medium (DMEM; Gibco, Carlsbad, CA) with the same additional supplements as listed above for MEM but with 10% dialyzed FCS (the same batch was used for all experiments) instead of standard FCS and the addition of 5.5 mM glucose or 10 mM galactose for the standard culture condition and the galactose-based stress medium, respectively.

## 2.2 | NMR spectroscopy

Sample preparation for <sup>1</sup>H-HR-MAS NMR was performed as described previously.<sup>15</sup> Briefly, 2.2 × 10<sup>6</sup> cells were seeded in 175 cm<sup>2</sup> flasks in GLC- or GAL-based medium and harvested after 18 h using trypsin–EDTA. Cells were pelleted (300 g, 5 min) and washed 3× with 1 mL PBS (pH 7.4). Cell pellets were resuspended in 35 µL D<sub>2</sub>O based 50 mM PBS (pD 7.0) to yield approximately 50 µL of total volume and subjected to three freeze–thaw cycles: 30 s in an ultrasonic bath at 50 Kc, 15 s in liquid N<sub>2</sub>. Cells were shock frozen and stored at –140°C until measuring day. The D<sub>2</sub>O based cell suspensions were heat inactivated (70°C, 20 min)<sup>15</sup> and transferred to a 4 mm standard zirconium rotor with a 50 µL insert. The rotor was weighed and transferred to a HR-MAS dual inverse <sup>1</sup>H/<sup>13</sup>C probe head in a 500 MHz Bruker Avance II spectrometer. Nominal temperature was 275 K, spinning speed 5 kHz at the magic angle of 54.7°. For each sample a PROJECTpr pulse sequence (1D <sup>1</sup>H T2-filter with presaturation)<sup>16</sup> was measured. Spectral width 5 kHz, 32k data size, 3.28 s acquisition time, TE 120 ms, 4 × 256 transients. The 90° pulse duration and the frequency of the water signal (O1) were determined for each sample. Spectral processing included line-broadening (1.0 Hz), phasing and baseline-correction. Samples were calibrated to the downfield peak of the lactate doublet (1.324 ppm). Spectral assignments were done using literature reference,<sup>17</sup> our own additional 2D correlation spectroscopy (<sup>1</sup>H<sup>1</sup>H-TOCSY) measurements and comparison with reference spectral databases (inhouse and the Human Metabolome Database, HMDB [LIT]). Three hundred and thirty buckets between 0.87 and 9.32 ppm were manually selected in Topspin while spectral regions without peaks and the water signal region were excluded. Total intensity normalization was used to account for differences in cell pellet volume while unit variance scaling was used to weight resonances from

metabolites with different concentrations the same. Upon spectral assignment of the individual metabolites, multiple buckets belonging to the same metabolite were merged to yield one value for each assigned metabolite. Principle component analysis (PCA), orthogonal partial least squares discriminant analysis (oPLS-DA), and individual metabolite analysis was performed with MatLab, PLS\_Toolbox (Eigenvector Research, Inc.) and Excel. For the individual metabolite analysis cell lines and replicates were merged into four groups: controls (10 Glc, 10 Gal), CI defects (9 Glc, 8 Gal), CV defects (6 Glc, 6 Gal), *MDH2* (4 Glc, 4 Gal), and subjected to a two-tailed *t*-test (homoscedastic, significance level of *p* < 0.01) and a subsequent Benjamini and Hochberg post-test (false discovery rate 0.25).

For determining the extracellular metabolome, a 450 µL aliquot of the spent cell culture media after 18 h incubation was measured with a 5 mm ATM BBFO probe upon the addition of 50 µL D<sub>2</sub>O based 50 mM PBS (pD 7.0) yielding 500 µL of total volume per 5 mm NMR tube. The same pulse sequence, parameters, and spectral processing steps were used as for the cell lysate samples. For every cell line at least three replicates were measured.

## 2.3 | Seahorse XFe96 metabolic flux analysis

We investigated metabolic flux in unbuffered culture medium using a Seahorse XFe96 cell analyzer. The oxygen consumption rate (OCR), an assessment of aerobic mitochondrial function, and extracellular acidification rate (ECAR), a detection of extracellular acid production, were measured simultaneously. Seven thousand cells/well were seeded on XFe96-well culture plates and were left to adhere overnight (timepoint 0). Per cell line and individual experiment and culture condition 22 cells were seeded. The next morning (timepoint 1) the cells were washed with PBS and incubated in GLC- or GAL-based medium for 17 h. The cells were incubated for an additional hour in unbuffered assay medium (DMEM, 5.5 mM glucose or 10 mM galactose, 2 mM L-glutamine, 1 mM sodium pyruvate, 100 U/mL penicillin, 100 µg/mL streptomycin, pH 7.4) at 37°C in a non-humidified, CO<sub>2</sub>-free incubator resulting in 18 h of total incubation time (timepoint 2). In parallel to seeding the 96 well plates per cell line and culture condition 210 000 cells/well (same seeding density) were seeded on two different six well plates. One plate was harvested after timepoint 1 and one plate after timepoint 2. Using a DC Protein Assay by BioRad the proliferation rate was then calculated. After establishing OCR and ECAR in basal respiration (i.e., the respiration prior to the addition of any

modulators) a Seahorse XF Cell Mito Stress Test profile was measured: ATP-linked respiration was determined by calculating the OCR delta upon addition of 1  $\mu\text{M}$  oligomycin, a CV inhibitor. 2.5  $\mu\text{M}$  carbonyl cyanide-p-trifluoromethoxy-phenylhydrazone (FCCP), an uncoupler, was used to achieve maximal respiration. Mitochondrial oxygen consumption was then halted by adding 1  $\mu\text{M}$  rotenone and 0.5  $\mu\text{M}$  antimycin A which inhibit CI and CIII, respectively. Background corrected OCR and ECAR data was normalized to cell number with the CyQuant assay (Thermo Fisher Scientific, Carlsbad, CA). The data was then normalized to the proliferation rate from the protein concentration thus accounting for cell growth and uneven plating during the experiment. For the calculation of specific steady-states, OCR was additionally corrected for non-mitochondrial oxygen consumption. Maximal respiration is defined as OCR under FCCP, while maximal acidification corresponds to ECAR under oligomycin. The respiratory spare capacity is calculated as the delta between maximum and basal respiration. For bioenergetic profile under basal respiration cell lines and replicates were merged into four groups: controls (9 Glc, 9 Gal), CI defects (4 Glc, 4 Gal), CV defects (4 Glc, 4 Gal), *MDH2* (3 Glc, 3 Gal). The means of these individual experiments were subjected to two-way ANOVA and a subsequent Bonferroni post-test (Table S4, adjusted  $p$ -value < 0.05). For the spare capacity the same statistical tests were applied but the defect cell lines were analyzed individually while the controls were merged (six groups, Table S5, adjusted  $p$ -value < 0.05). When comparing the glucose spare capacity of a cell line with its galactose spare capacity two-way ANOVA was used (one group, Table S5,  $p$ -value < 0.05).

### 3 | RESULTS

#### 3.1 | Bioenergetic analysis

Incubation of all measured cell lines in galactose condition led to an expected shift from glycolytic towards aerobic metabolism (Figure 1). This was observed as a decrease in extracellular acidification rate and an increase of oxygen consumption rate.

In the glucose-based condition the mean basal respiration of the control fibroblasts was significantly higher ( $p < 0.05$ ) than the mean respiration of CI, and CV deficient cells but not significantly higher than the mean respiration of *MDH2* deficient cells (cf. Table S4 for  $p$ -values). The respiratory spare capacity of either CI defect under glucose condition was significantly lower compared to controls (Figure 2, Table S5 for  $p$ -values).

#### Bioenergetic Profile basal condition

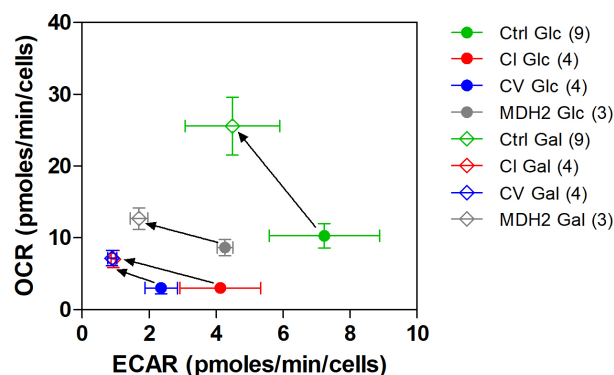


**FIGURE 1** Bioenergetic profiling at basal state after 18 h incubation in glucose (Glc) and galactose (Gal) based condition. Values represent the mean  $\pm$  SEM ( $n = \#$  of independent experiments shown in brackets in the legend). The controls are the average of three cell lines, CI and CV of two cell lines, respectively while *MDH2* is one cell line. Data points connected by arrows highlight the shift of basal OCR and ECAR from glucose towards galactose condition for each cell line used. Statistical tests are in Table S4.

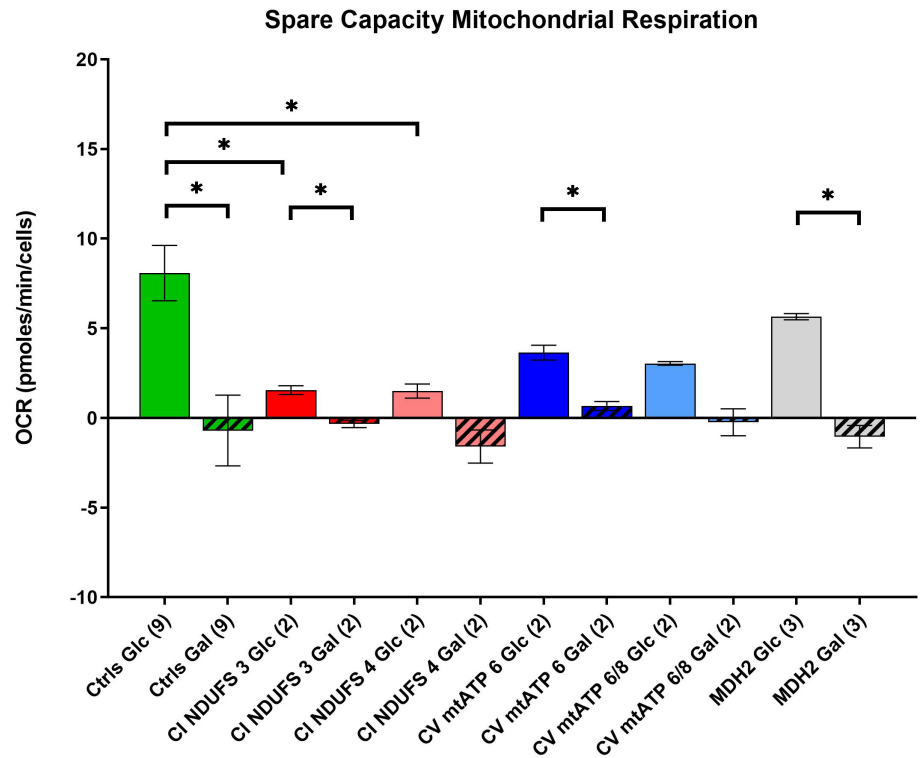
Under glucose condition both complex I defects showed the lowest spare capacity followed by both complex V defects with *MDH2* having the highest spare capacities of the studied defects.

Under galactose, the differences in basal respiration between controls and defects were not statistically significant (Table S5). For all measured cell lines, the spare capacity was close to zero for all cell lines measured under galactose indicating that the cells were respiring maximally.

#### 3.2 | Supernatant metabolomes

Chemometric analysis of NMR based cell supernatants revealed a strong separation of controls from defects for both PCA and oPLS-DA under glucose and galactose condition, respectively, with no clear improvement for the galactose condition (Figure S3). Separation of defects from each other was not achieved. Under glucose condition defects showed higher concentrations of lactate, glutamine, alanine and uracil and lower concentration of several amino acids (phenylalanine, leucine, isoleucine, and valine), creatine, and pyruvate when compared to controls (Table S6). Under galactose condition most metabolites showed a similar pattern, however, lactate was no longer a strong driver for separating controls from defects and had overall a lower concentration. Pyruvate on the other hand, switched to being increased in defects relative to controls.

**FIGURE 2** Cell line specific spare capacity after 18 h incubation in glucose and galactose based condition. Values represent the mean  $\pm$  SEM ( $n = \#$  of independent experiments shown on  $x$ -axis). The controls are the average of three cell lines measured as triplicates. Values are from at least two independently measured biological replicates with an average of 17 selected wells per experiment (technical replicates). Statistical significance versus controls is shown as:  $*p < 0.05$ . Slightly negative values depicted in this figure are due to measuring inaccuracies of the Seahorse analyzer (as maximal respiration cannot be lower than the basal respiration). Statistical tests are in Table S5.



### 3.3 | Cellular metabolomes

Forty and 38 metabolites were determined for the glucose and galactose condition, respectively and used for chemometric analyses (Figure S1). Unbiased PCA demonstrated close clustering of replicates, especially in galactose condition (Figure 3A,B). Main separation was obtained between controls and *MDH2* along PC1, while CI and CV cluster in between, which was again more pronounced in galactose. In galactose condition PC2 separated mostly the different replicates, possibly indicating secondary variances within cell lines. Supervised oPLS-DA was performed twice, first treating each cell line as its own group (3 control, 2 CI, 2 CV, and 1 *MDH2*). Similar to PCA, the first latent variable (LV) separates the controls well from *MDH2* with CI and CV defects falling in between, especially for galactose condition (Figure 3C,D). CI and CV were not separated. While within groups no separation was obtained along LV1, higher LVs separated again mostly the individual cell lines, however, without demonstrating significant separation in permutation tests. To test the possibility to merge the three control lines and separately the CI and CV defects for the following comparison of individual metabolites between groups, oPLS-DA was also performed on the four merged groups, that is, controls, CI, CV, and *MDH2* (Figure 3E,F). While the separation along LV1 remains, the intra-group separation is lost, supporting the merge for the individual metabolite

analysis. However, it remains possible that also within CI and CV defects metabolic differences exist, leading to the separation in the PCA and the first oPLS-DA. Permutation tests revealed significant separation of the merged control group and *MDH2* from all other groups in both, glucose and galactose condition (Tables S2 and S3). The permutation results indicate in addition a trend for CV to be separated in galactose condition, only (Table S3).

In addition to the oPLS-DA analysis of the merged groups, a two-tailed  $t$ -test ( $p$  value  $< 0.01$ ) with Benjamini Hochberg post-test for all selected metabolites was done between *NDUFS3* versus *NDUF4* and *mtATP6* versus *mtATP6/8* to check for intra-group variances. Malate was one of very few significant metabolites being increased in *NDUFS3* (relative to *NDUFS4*) under galactose but decreased under glucose (relative to *NDUFS4*). It was, therefore, decided to merge the complex I and V cell lines for the individual metabolite plots, which also increased the statistical power (Figure 4).

Under glucose culture condition the branched chain amino acids valine, isoleucine, and leucine were lower in *MDH2* compared to CI and CV (Figure 4A). Fumarate was elevated in *MDH2* compared to controls. Malate was increased in controls compared to CI (Figure 4B). NAD<sup>+</sup> and UMP were significantly decreased in all defects relative to controls (Figure 4C). Creatinine was elevated in *MDH2* but not in the OXPHOS defects (Figure 4E). Conversely, *MDH2* showed decreased phenylalanine, tyrosine, and glutamate levels relative to other defects

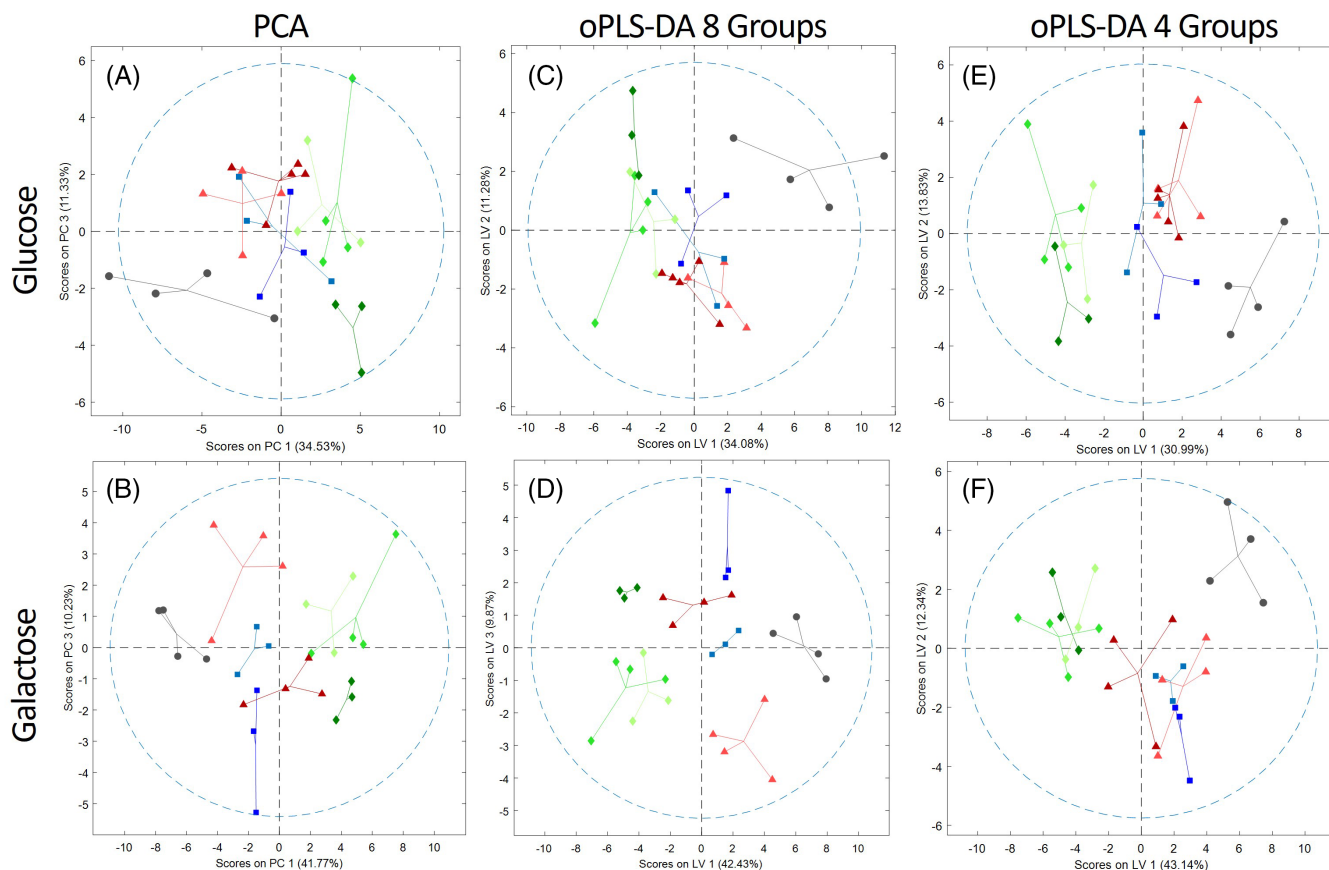


**FIGURE 3** Chemometric analysis of intracellular metabolites in glucose versus galactose based condition. Unbiased PCA and supervised oPLS-DA of glucose and galactose condition, respectively. Eight-group-plots treat every cell line individually, while four-group plots merge the three controls, the two CI and the two CV cell lines. Mean center and unit variance scaling was used for all plots. Connected dots show biological replicates of the same cell line. Controls  $\bullet$ , CI  $\blacktriangle$ , CV  $\blacksquare$ , and MDH2  $\bullet$ .

and controls under glucose. Inositol and creatine were strongly upregulated in all defects and in both conditions (Figure 4D,E). Galactose-1-phosphate (Gal-1-P), a metabolite of the galactose catabolism, could only be detected under galactose culture condition and was significantly lower in *MDH2* relative to controls. Under galactose culture condition alanine was decreased in *MDH2* compared to controls while valine and isoleucine were decreased in both CV and *MDH2* but not CI. Aspartate was elevated in both OXPHOS defects but not in *MDH2* (Figure 4A) whereas glutamate was only decreased in *MDH2*. Acetate, NAD<sup>+</sup>, UMP, glycerol-phosphocholine (GPC), and UDP-N-acetyl-glucose all were found to be decreased in all defects relative to controls (Figure 4A–E). Uracil showed a stark increase in *MDH2* relative to all other cell lines while CI and CV were decreased relative to controls (Figure 4C). Methylene groups of lipids, which make up the saturated part of a fatty acids, were only increased in *MDH2* while terminal methyl groups of lipids were decreased in CI and *MDH2* relative to controls (Figure 4D). Although no individual metabolite was significantly different between CI and CV after correcting for multiple comparisons, our data

indicated certain amino acids (valine, isoleucine, phenylalanine, and tyrosine), and malate as potential metabolites separating mitochondrial CV from CI defects primarily in galactose condition (Figure S2). For differentiating *MDH2* from the respiratory chain defects and controls inositol and most amino acids proved significant.

## 4 | DISCUSSION

We studied the metabolic signatures of five HSF lines with mitochondrial defects using NMR and metabolic flux analysis. Our hypothesis that selective galactose culture would cause defect specific adaptations of the metabolome proved correct for *MDH2* and to a lesser extent for CI and CV. The extracellular metabolome provided separation between defects and controls, whereas the intracellular metabolome suggested CI and CV changes and revealed clear *MDH2* defect-specific changes in metabolites associated with the TCA cycle, malate aspartate shuttle and the choline metabolism, which were more pronounced under galactose condition.

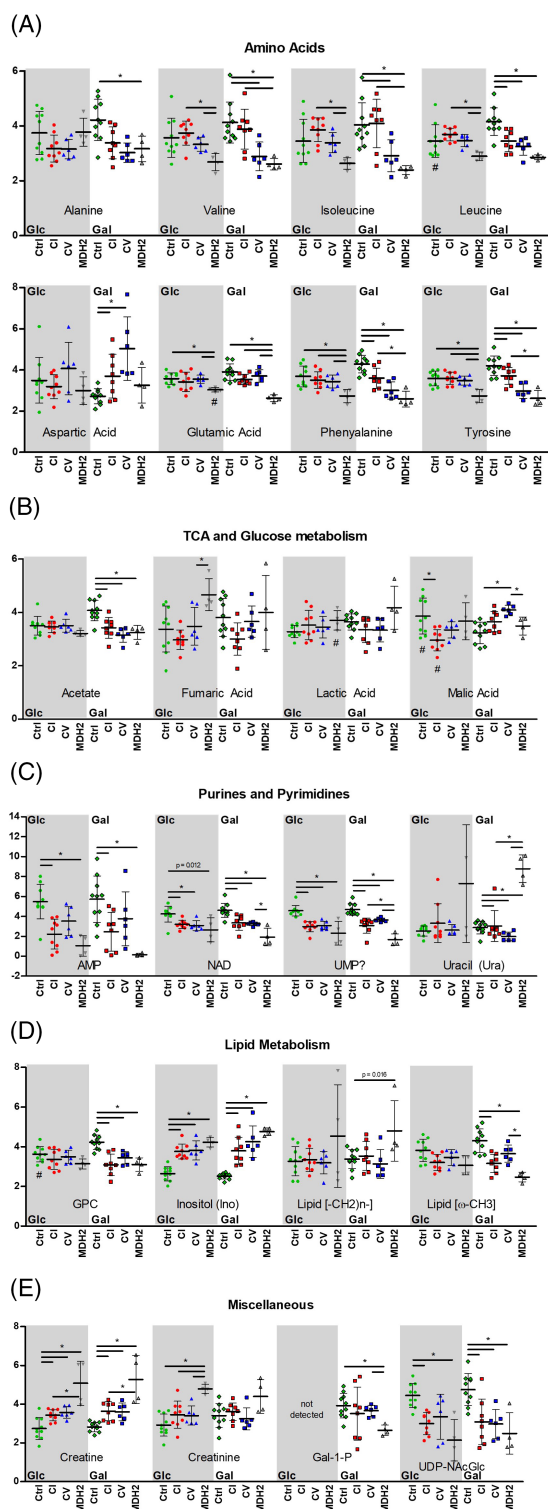


**FIGURE 4** Quantitative analysis of intracellular metabolites using  $^1\text{H}$  HR-MAS NMR. Ctrl, CI, CV, and MDH2 deficient fibroblasts were cultured in glucose or galactose based medium for 18 h. (A–E) In total, 24 of 40 assigned metabolites showed significant differences either between controls, CI, and CV defective cell lines ( $*p < 0.01$ ) or between glucose and galactose condition within the cell line group ( $\#p < 0.01$ ). The horizontal line shows which two groups are being compared. The y-axis is normalized to the average intensity of the glucose cultured control group.  $p$  values slightly greater than 0.01 are denoted as such.

## 4.1 | Bioenergetic analysis

In all measured cell lines, the galactose culture condition led to bioenergetic switch from a glycolytic to oxidative state (Figure 1) and resulted in a spare capacity close to zero (Figure 2), indicating that all cells were respiring maximally, and the deficient pathways were maximally stressed. This led to an improved separation between groups (Figure 3) as further discussed below in the chemometric analysis.

When comparing the basal respiration of the different defects MDH2 had a slightly higher oxygen consumption rate than the OXPHOS defects for both glucose and galactose condition. Since the MDH2 defect have an intact OXPHOS its bioenergetic issues lie in the production and transportation of reducing equivalents (NADH) not in their oxidation via OXPHOS.

Although not statistically significant the spare capacity for both CV defects under glucose were higher when compared to either CI defect. The complex V defect *mtATP6* has been previously described to have a low ability to use its respiration generated proton gradient for ATP synthesis which results in a high membrane potential.<sup>18</sup> Once uncoupled, during the mito stress test, the respiration is no longer limited by the ATP synthase which in turn might lead to an overestimation of the spare capacity as these mitochondria do not have the ability to convert this capacity into ATP production. High membrane potential (hyperpolarization) is endemic in complex V defects and results in a high production of ROS<sup>19,20</sup> which plays a major role in pathophysiological signal transduction affecting many metabolic pathways.

## 4.2 | Chemometric analysis of NMR based metabolomes

As described in Section 3 of the NMR based cell supernatant metabolomes lactate proved a strong driver for separating the studied defects from controls. This is in good agreement with the literature which reports that elevated lactate levels in the plasma have been observed in the defects studied within the scope of this paper.<sup>21–24</sup> However, many mitochondrial disorders do not present with elevated lactate or only during a metabolic crisis, thus making lactate an unreliable marker for differential diagnosis.<sup>25</sup> This underlines the usefulness of metabolomic analysis of cell homogenates as the observed differences from supernatants are not defect specific.

When analyzing the cellular metabolomes PCA and oPLS-DA showed clear separation of controls, OXPHOS defects and MDH2 along the principal axis (Figure 3). The fact that MDH2 is not part of the oxidative chain

suggests itself as the reason for its clear separation from CI and CV (Figure 3). While no single metabolite was significantly different on its own when comparing CI and CV defects, Figure 3E shows clustering of individual complex I (*NDUFS3*, *NDUFS4*) and complex V (mtATP 6, mtATP 6/8) under galactose condition. Relative to complex I several amino acids (alanine, valine, isoleucine, phenylalanine, and tyrosine) were lower in complex V while malate, fumarate, and aspartate were found to be increased when used in an oPLS-DA analysis of complex I and V (Figure S2) as can also be derived from Figure 4. It has been shown that complex I inhibition in the presence of succinate drives complex II respiration.<sup>26</sup> This could explain the decreased malate, fumarate, and aspartate (via oxaloacetate by MDH2 and GOT2) levels in complex I relative to complex V. This demonstrates the usefulness of multivariate analysis and selective culture condition for detecting differences among closely related defects.

Figure 4D shows that inositol was strikingly increased in all studied defects regardless of the culture condition. Inositol is a ubiquitous metabolite which is involved in many signaling pathways linked to apoptosis, cell growth, and many more.<sup>27</sup> Hsu et al.<sup>28</sup> studied inositol monophosphatase deficient cells and were able to show that inositol restricts AMPK activation and mitochondrial fission. They suggest, that since inositol competes with AMP for AMPK the AMP/inositol ratio is key for determining AMPK activity and thus AMPK-dependent mitochondrial fission. Our data shows significantly increased inositol for all defects compared to controls while AMP was generally decreased relative to controls. Since reduced mitochondrial fission is linked to impaired energy metabolism<sup>29</sup> it is possible that the measured inositol and AMP levels in defects are reflective of the reduced OXPHOS activity observed in all defects (cf. OCR levels in Figure 1).

NAD<sup>+</sup> was significantly decreased in *MDH2* versus controls (cf. Figure 4C). As *MDH2* defects are hindered in their ability to oxidize malate to oxaloacetate in their mitochondria this leads to an interruption of the TCA cycle and the malate aspartate shuttle (MAS). A deficient MAS affects the cytosolic NAD<sup>+</sup>/NADH redox balance as the indirect transport of NADH across the mitochondrial membrane via malate no longer works.<sup>30</sup> It is therefore possible that the exceptionally low NAD<sup>+</sup> measured in *MDH2* defective cells results from an inability to indirectly transport NADH at the usual rate into the mitochondria where NAD<sup>+</sup> could be regenerated via complex I. So far, we were unable to measure NADH as its concentration, depending on the cellular compartment, is between 10 times and several 100 times lower than NAD<sup>+</sup>.<sup>31</sup> Therefore, comparisons of NAD<sup>+</sup>/NADH ratios between cell lines are difficult unless a constant NAD<sup>+</sup>/NADH pool is assumed.

Fumarate was significantly increased for *MDH2* under glucose (Figure 4B). There are reports in literature of subjects with at least one allele exhibiting the same c.398C>T mutation showing increased fumarate in fibroblasts.<sup>32</sup> Elevated fumarate, measured in *MDH2* KO cells<sup>33</sup> and reported in urinary organic acid analysis, is also one of the non-specific biomarkers mentioned by Broeks et al.<sup>30</sup> in their comprehensive review on inborn errors of the malate aspartate shuttle. However, malate was not found to be increased significantly under either culture condition which hints at a more complex cause than fumarate just being upstream of MDH2 in the TCA cycle.

When comparing lipid levels (cf. Figure 4D) under galactose culture condition *MDH2* defects showed increased concentrations ( $p = 0.016$ ) of methylene groups,  $(-\text{CH}_2-)_n$ , and significantly decreased concentrations of terminal methyl groups,  $\omega\text{-CH}_3$ , relative to controls. Assuming a similar pool of total lipids this indicates that on average the measured *MDH2* deficient cells had more of longer fatty acid chains than controls in their lipids. Glycerophosphocholine (GPC) was found to be decreased in all defects under galactose condition. Interestingly, the same was observed in our previous study when characterizing a pyruvate dehydrogenase defect.<sup>9</sup> GPCs may be indicative of a secondary disturbance of the Kennedy pathway. The Kennedy pathway (CDP-choline pathway) is meant to be the predominant mechanism for phosphatidylcholine synthesis<sup>34</sup> and is known to play a role in choline-related-inherited metabolic diseases.<sup>35</sup> Albeit not statistically significant, both choline and phosphocholine (PC) were elevated in all defects when compared to controls under galactose condition but not under glucose condition (data not shown). In our previous study we observed significantly increased levels of choline, and PC in CI defects (*ND6* and *NDUFAF2*)<sup>36</sup> in both culture conditions while GPC was not significantly changed relative to controls. Our *NDUFS3* and *NDUFS4*<sup>36</sup> defects pertain to the iron-sulfur proteins which shuttle electrons while *ND6* encodes a protein pumping subunit and *NDUFAF2* encodes an assembly factor. These specific CI defects could potentially affect the choline pathways differently, but the, partially significant, increase in choline and PC in all CI defects is noteworthy.

## 5 | CONCLUSION

This preliminary metabolomics HR-MAS NMR study indicates the benefit of using galactose versus standard culture conditions providing better separation and insights into disturbed oxidative metabolism by respiratory chain disorders. Results suggest CI and CV defect specific metabolic adaptations in human fibroblasts.



## AUTHOR CONTRIBUTIONS

**Christoph Meyer, Damian Hertig, Janine Arnold, Christian Urzi, Sandra Kurth, Peter Vermathen, and Jean-Marc Nuoffer** conceived the work and designed the experiments. **Christoph Meyer, Janine Arnold, Christian Urzi, and Sandra Kurth** cultured cells, performed metabolic flux experiments and analyzed the data. **Christoph Meyer, Janine Arnold, and Damian Hertig** performed NMR analysis of cells or supernatant and analyzed the data. **Johannes A. Mayr** provided the cells. **Peter Vermathen and Jean-Marc Nuoffer** provided experimental advice and overall guidance. **André Schaller** provided the genetic characteristics of the patient fibroblast. **Christoph Meyer, Johannes A. Mayr, André Schaller, Peter Vermathen, and Jean-Marc Nuoffer** wrote the manuscript or revised it critically for important intellectual content. All authors approved the final manuscript.

## FUNDING INFORMATION

This work was supported by Swiss National Science Foundation SNF grant (192691 Peter Vermathen and Jean-Marc Nuoffer).

## CONFLICT OF INTEREST STATEMENT

All authors have declared no conflicts of interest.

## DATA AVAILABILITY STATEMENT

The data that support the findings of this study are available from the corresponding author upon reasonable request.

## ETHICS STATEMENT

All procedures performed in studies involving human participants were in accordance with the 1975 Helsinki declaration and its later amendments and approved by the Ethics Committee of the University Hospital of Bern.

## INFORMED CONSENT

Informed consent was obtained from all individual participants included in the study.

## ANIMAL RIGHTS

This article does not contain any studies with animal subjects performed by any of the authors.

## ORCID

**Christoph Meyer**  <https://orcid.org/0009-0000-6010-300X>  
**Damian Hertig**  <https://orcid.org/0000-0002-0141-1691>  
**Peter Vermathen**  <https://orcid.org/0000-0001-8649-1098>  
**Jean-Marc Nuoffer**  <https://orcid.org/0000-0003-3650-6153>

## REFERENCES

- Finsterer J, Zarrouk-Mahjoub S. Biomarkers for detecting mitochondrial disorders. *J Clin Med*. 2018;7:16.
- Chandel NS. Mitochondria as signaling organelles. *BMC Biol*. 2014;12:1-7.
- Poveda-Huertes D, Taskin AA, Dhaouadi I, et al. Increased mitochondrial protein import and cardiolipin remodelling upon early mtUPR. *PLoS Genet*. 2021;17:e1009664.
- Chandel NS, Maltepe E, Goldwasser E, Mathieu CE, Simon MC, Schumacker PT. Mitochondrial reactive oxygen species trigger hypoxia-induced transcription. *Proc Natl Acad Sci U S A*. 1998;95:11715-11720.
- Thelen MP, Wirth B, Kye MJ. Mitochondrial defects in the respiratory complex I contribute to impaired translational initiation via ROS and energy homeostasis in SMA motor neurons. *Acta Neuropathol Commun*. 2020;8:1-19.
- He Y, Leung KW, Zhang YH, et al. Mitochondrial complex I defect induces ROS release and degeneration in trabecular meshwork cells of POAG patients: protection by antioxidants. *Invest Ophthalmol Vis Sci*. 2008;49:1447-1458.
- Bustamante E, Pedersen PL. High aerobic glycolysis of rat hepatoma cells in culture: role of mitochondrial hexokinase. *Proc Natl Acad Sci U S A*. 1977;74:3735-3739.
- Aguer C, Gambarotta D, Mailloux RJ, et al. Galactose enhances oxidative metabolism and reveals mitochondrial dysfunction in human primary muscle cells. *PLoS One*. 2011;6:e28536.
- Hertig D, Felser A, Diserens G, Kurth S, Vermathen P, Nuoffer JM. Selective galactose culture condition reveals distinct metabolic signatures in pyruvate dehydrogenase and complex I deficient human skin fibroblasts. *Metabolomics*. 2019;15:32.
- Zhang S, Nagana Gowda GA, Ye T, Raftery D. Advances in NMR-based biofluid analysis and metabolite profiling. *Analyst*. 2010;135:1490-1498.
- Lindon JC, Beckonert OP, Holmes E, Nicholson JK. High-resolution magic angle spinning NMR spectroscopy: application to biomedical studies. *Prog Nucl Magn Reson Spectrosc*. 2009;55:79-100.
- Levitt MH. *Spin Dynamics: Basics of Nuclear Magnetic Resonance*. John Wiley & Sons, Ltd.; 2008.
- Power WP. High-resolution magic angle spinning—enabling applications of NMR spectroscopy to semi-solid phases. *Annu Reports NMR Spectrosc*. 2011;72:111-156.
- Laemmle A, Steck AL, Schaller A, et al. Triheptanoin—novel therapeutic approach for the ultra-rare disease mitochondrial malate dehydrogenase deficiency. *Mol Genet Metab Reports*. 2021;29:100814.
- Diserens G, Hertig D, Vermathen M, et al. Metabolic stability of cells for extended metabolomic measurements using NMR. A comparison between lysed and additionally heat inactivated cells. *Analyst*. 2017;142:465-471.
- Aguilar JA, Nilsson M, Bodenhausen G, Morris GA. Spin echo NMR spectra without J modulation. *Chem Commun*. 2012;48:811-813.
- Vermathen M, Paul LEH, Diserens G, Vermathen P, Furrer J. 1H HR-MAS NMR based metabolic profiling of cells in response to treatment with a hexacationic ruthenium metal-lapirism as potential anticancer drug. *PLoS One*. 2015;10:e0128478.

18. Houšťek J, Pícková A, Vojtišková A, Mráček T, Pecina P, Ješina P. Mitochondrial diseases and genetic defects of ATP synthase. *Biochim Biophys Acta - Bioenerg.* 2006;1757:1400-1405.
19. Korshunov SS, Skulachev VP, Starkov AA. High protonic potential actuates a mechanism of production of reactive oxygen species in mitochondria. *FEBS Lett.* 1997;416:15-18.
20. Forrester SJ, Kikuchi DS, Hernandez MS, Xu Q, Griendling KK. Reactive oxygen species in metabolic and inflammatory signaling. *Circ Res.* 2018;122:877-902.
21. Haas RH et al. The in-depth evaluation of suspected mitochondrial disease. *Mol Genet Metab.* 2008;94:16-37.
22. Rahman S, Blok RB, Dahl HHM, et al. Leigh syndrome: clinical features and biochemical and DNA abnormalities. *Ann Neurol.* 1996;39:343-351.
23. Alston CL, Rocha MC, Lax NZ, Turnbull DM, Taylor RW. The genetics and pathology of mitochondrial disease. *J Pathol.* 2017;241:236-250.
24. Kirby DM, Crawford M, Cleary MA, Dahl HHM, Dennett X, Thorburn DR. Respiratory chain complex I deficiency. *Neurology.* 1999;52:1255-1264.
25. Debray FG, Mitchell GA, Allard P, Robinson BH, Hanley JA, Lambert M. Diagnostic accuracy of blood lactate-to-pyruvate molar ratio in the differential diagnosis of congenital lactic acidosis. *Clin Chem.* 2007;53:916-921.
26. Molinié T, Cougouilles E, David C, Cahoreau E, Portais JC, Mourier A. MDH2 produced OAA is a metabolic switch rewiring the fuelling of respiratory chain and TCA cycle. *Biochim Biophys Acta - Bioenerg.* 2022;1863:148532.
27. Ritter SL, Hall RA. Fine-tuning of GPCR activity by receptor-interacting proteins. *Nat Rev Mol Cell Biol.* 2009;10:819-830.
28. Hsu C-C, Zhang X, Wang G, et al. Inositol serves as a natural inhibitor of mitochondrial fission by directly targeting AMPK. *Mol Cell.* 2021;81:3803-3819.e7.
29. Aksu-Menges E, Eylem CC, Nemetlu E, et al. Reduced mitochondrial fission and impaired energy metabolism in human primary skeletal muscle cells of megaconial congenital muscular dystrophy. *Sci Rep.* 2021;11:18161.
30. Broeks MH, van Karnebeek CDM, Wanders RJA, Jans JJM, Verhoeven-Duif NM. Inborn disorders of the malate aspartate shuttle. *J Inherit Metab Dis.* 2021;44:792-808.
31. Yang Y, Sauve AA. NAD<sup>+</sup> metabolism: bioenergetics, signaling and manipulation for therapy. *Biochim Biophys Acta.* 2016;1864:1787-1800.
32. Ait-El-Mkadem S, Dayem-Quere M, Gusic M, et al. Mutations in MDH2, encoding a Krebs cycle enzyme, cause early-onset severe encephalopathy. *Am J Hum Genet.* 2017;100:151-159.
33. Cascón A, Comino-Méndez I, Currás-Freixes M, et al. Whole-exome sequencing identifies MDH2 as a new familial paraganglioma gene. *J Natl Cancer Inst.* 2015;107:53.
34. Tavasoli M, Lahire S, Reid T, Brodovsky M, McMaster CR. Genetic diseases of the Kennedy pathways for membrane synthesis. *J Biol Chem.* 2020;295:17877-17886.
35. Wortmann SB, Mayr JA. Choline-related-inherited metabolic diseases—a mini review. *J Inherit Metab Dis.* 2019;42:237-242.
36. HGNC. *Mitochondrial complex I: NADH:ubiquinone oxidoreductase subunits.* <https://www.genenames.org/data/genegroup/#!/group/640> (2023).

## SUPPORTING INFORMATION

Additional supporting information can be found online in the Supporting Information section at the end of this article.

**How to cite this article:** Meyer C, Hertig D, Arnold J, et al. Complex I, V, and MDH2 deficient human skin fibroblasts reveal distinct metabolic signatures by <sup>1</sup>H HR-MAS NMR. *J Inherit Metab Dis.* 2023;1-10. doi:10.1002/jimd.12696